IEEE Access
Multidisciplinary | Rapid Review | Open Access Journal

Received 23 January 2024, accepted 5 February 2024, date of publication 13 February 2024, date of current version 8 March 2024.

Digital Object Identifier 10.1109/ACCESS.2024.3365781

RESEARCH ARTICLE

A Sensorless Control Method for Energy Recovery of EGTAC to Improve PEMFC Efficiency

LIJIANG JIN[1], JICHENG XU[2], AND LINZHI WANG[1]

[1]School of Transportation, Zhenjiang College, Zhenjiang 212028, China
[2]Jiangsu Province Engineering Research Center of Surface Interface Functional Composites, Institute of Chemistry and Materials Science, Zhenjiang College, Zhenjiang 212028, China

Corresponding author: Lijiang Jin (jin_lijiang@163.com)

This work was supported in part by Zhenjiang Science and Technology Innovation Key Research and Development Plan, in 2020, under Grant SH2020010.

ABSTRACT The efficient operation of the air supply system, particularly the air compressor, is crucial in ensuring the performance of the proton exchange membrane fuel cells (PEMFCs). Nevertheless, its high parasitic power consumption is the main reason for the efficiency decline of the PEMFC. While exhaust gas energy recovery is a viable approach to enhance system efficiency, conventional exhaust gas recovery systems are not well-suited for PEMFC and the cathode exhaust gas is difficult to monitor in real-time. Therefore, this study proposes a sensorless method based on reinforcement learning for energy recovery of the exhaust gas turbine air compressor (EGTAC) in the PEMFC. Firstly, the air supply system with EGTAC and stack model are established. Subsequently, the relationship between the exhaust gas energy and the working performance of both the EGTAC and the PEMFC is elucidated. Additionally, a method based on a state observer is devised to estimate the characteristics of the exhaust gas in a PEMFC. Finally, compared to the model predictive control (MPC), this method enhances the EGTAC exhaust gas recovery rate by 19.1% and the fuel cell system efficiency by 3.7%. The optimization differs by a maximum of 6.5% compared to the control with sensors.

INDEX TERMS Exhaust gas energy recovery, estimation of exhaust gas characteristics, reinforcement learning, sensorless control.

I. INTRODUCTION

In past few years, as the problems of energy scarcity and environmental degradation are becoming more and more apparent, countries all over the world have begun to search for new clean energy sources as substitutes for fossil energy sources and are actively exploring low carbon and high efficiency energy development routes. Hydrogen, as a secondary energy carrier, has been widely recognized and paid attention to because of its many advantages, like high efficiency, renewability, and stable energy conversion process [1], [2], [3]. PEMFCs, which utilizes hydrogen as its primary fuel, has increasingly gained attention and is seen as one of the most promising technologies to replace conventional internal combustion engines as the power source for vehicles in the future [4], [5], [6], [7]. The air supply system plays a crucial role in the PEMFC, in which the core component, the air compressor is in charge of supplying air to the fuel cell so that hydrogen and oxygen may react to produce energy and water. For higher power density and better performance, the PEMFC must operate at higher pressures, usually in the range of 2.0 to 2.5 atmospheres or so [8], [9]. Therefore, it is necessary for the air supply to promptly adapt to the change of load.

Some scholars used a variety of methods [10], [11], [12], [13], [14] to control and optimize the intake of the air supply system, which have achieved good results and improved the fuel cell's performance, but ignored the power loss of the air compressor. When the input pressure rises, the power of PEMFC increases, and the power consumption of air compressor will also be higher [15], [16], [17]. It is imperative that the air supply system's power consumption be

The associate editor coordinating the review of this manuscript and approving it for publication was Xiaosong Hu.

decreased, and that the overall efficiency of fuel cell system be increased. Several scholars have enhanced the efficiency of fuel cell systems by using energy management strategies [18], employing multi-objective optimization control strategies [19], and other methods. Recycling the system's exhaust energy is a mature method of increasing system efficiency [20]. Exhaust energy recovery has been a topic of active discussion in the research field of conventional engine vehicles and hybrid electric vehicles. This method improved the dynamic performance and economic performance of engine [21], [22].

Compared to the traditional engine vehicle, the fuel cell vehicles (FCVs) also have a large amount of available energy, such as the energy of the cathode outlet gas, the pressure energy in the hydrogen storage bottle and the waste heat energy of the radiator. Unused energy is discharged into the surrounding environment, accounting for nearly 50% of the total energy loss [23], [24]. Pei et al. [25] analyzed the effect of different connection forms of exhaust gas energy recovery device on the fuel cell system. In order to determine the best course and optimization direction for optimizing future twin-screw expanders for fuel cells, Wang et al. [26] investigated the operating characteristics of the expander installed at the cathode of the electric reactor under various working situations and geometries. Wei et al. [27] simulated the exhaust gas energy recovery process of fuel cells under different operating loads, and obtained the effects of inlet state, current density, etc. on the turbine recovery efficiency. It offers a foundation for researching the best ways to govern exhaust gas recovery. Santiago [28] et al proposed an optimization method for electrically assisted coupled turbine structure and designed a decoupling control method for air compressor and turbine to improve the turbine efficiency, however, the increase of electrical losses reduces the efficiency of the whole system. Li et al. [29] established a model of the exhaust gas recovery system of PEMFC by controlling the air excess rate to supply the air flow, and the outcomes of the simulation demonstrated that this technique may raise the system power by 13%. However, the turbine's power contributed to 18% of the total parasitic power consumption. Thus, while utilizing a turbine to recover energy can enhance the power performance and economy of PEMFC, it increases additional power consumption and requires a certain amount of time to reach operational status. Additionally, the turbine's response time is sluggish, which fails to meet the immediate gas supply demands of the fuel cell system [30], [31]. Therefore, there is growing interest in the fuel cell air compressor that can directly recover the cathode exhaust gas, necessitating more research and development of its exhaust gas recovery optimization control.

In addition, the above scholars' research on the cathode exhaust gas energy recovery system largely depends on the continuous monitoring of the cathode gas concentration to maintain the gas condition at the desired level. Nevertheless, the installation of a sensor at the cathode outlet of the stack to measure cathode exhaust gas parameters is both expensive and difficult to install [32]. Additionally, the low temperature at the cathode outlet of the stack generates a significant quantity of water vapor, which diminishes the precision and responsiveness of the sensor [33]. The fuel cell is also susceptible to metal ions, leading to a diminished reliability of the sensor [34]. While the mass spectrometer can be employed for precise diagnosis and analysis of gas concentration, the closed structure of the PEMFC system necessitates modifications to the fuel cell stack. Specifically, this involves the insertion of a capillary gas sampling tube into the flow channel, resulting in increased complexity and cost. Furthermore, the mass spectrometer exhibits a notably prolonged response time to water vapor pressure. This, in turn, leads to dynamic alterations in the internal operational state of the fuel cell, ultimately yielding measurement findings that are deemed inaccurate [35], [36]. Thus, it is imperative to create an observer that relies on a precise model of the fuel cell system and observable signals. This will ensure that the predicted gas concentration aligns with the actual value and enable real-time estimation of exhaust characteristics [37]. Based on the above, the structure of the paper is illustrated in Figure 1 and the contributions of this paper are as follows:

(1) This study proposes an accurate estimation method of fuel cell cathode exhaust characteristics based on the observer to solve the problem that it is difficult to monitor the cathode outlet gas of the fuel cell system in real-time. The change of working characteristics of the air supply system and fuel cell system caused by the change of exhaust energy was explored.

(2) This study proposes a novel fuel cell air compressor that incorporates an exhaust gas recovery feature to efficiently recover and process the cathode exhaust gas from fuel cells, therefore streamlining the exhaust gas energy recovery system. A control method utilizing a reinforcement learning algorithm is developed to enhance the efficiency of exhaust gas recovery and fuel cell system, without the need for sensors.

II. MODELING

This paper uses a mechanism modeling approach to establish the mathematical model of a PEMFC stack and air supply system. The assumptions are as follows: (1) It is assumed that the ideal gas law applies to all gases. (2) It is assumed that the internal temperature distribution of the stack is balanced and that the gas temperature of the electrode and the stack are equal. (3) It is assumed that the hydrogen flow is sufficient and the hydrogen pressure meets the requirements of the following air pressure.

A. FUEL CELL STACK MODEL

Through the principle of electrochemistry, the stack model shows the output performance of the battery, and uses the law of conservation of matter to show the dynamic change of gas mass flow in the cathode flow field. By means of empirical and physical formulas, such as concentration polarization

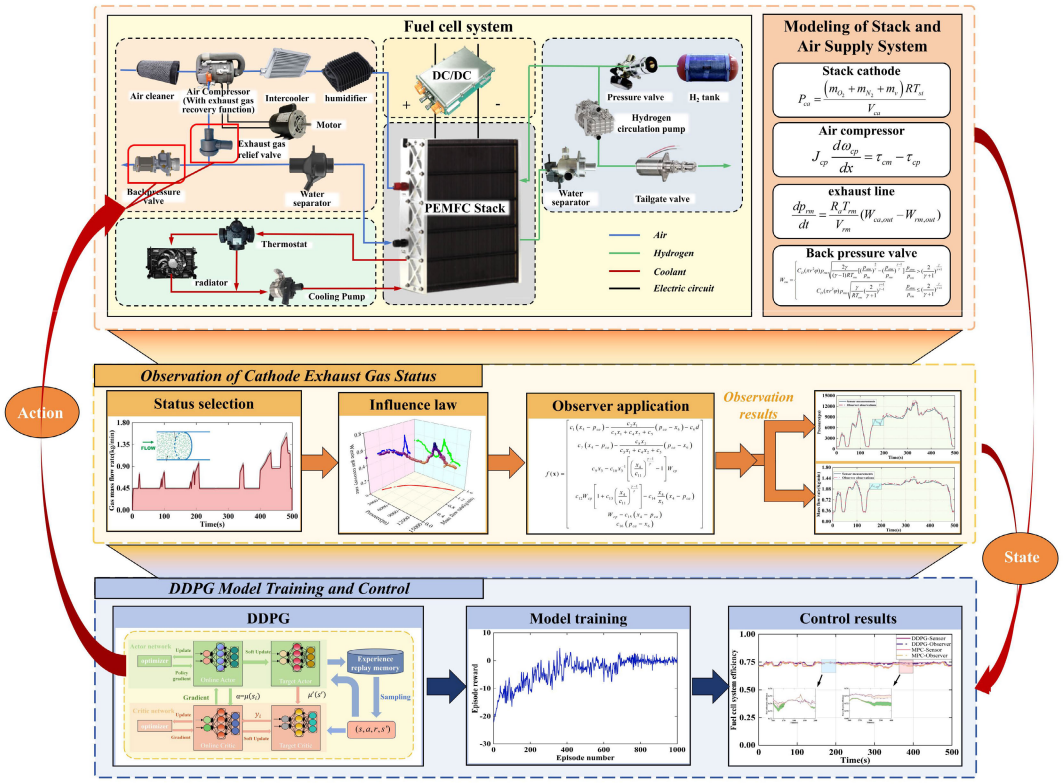

FIGURE 1. Framework of this paper.

voltage, ohmic polarization voltage, activation polarization voltage, and Nernst voltage, the fuel cell's output voltage model expresses the output characteristics of the stack [38]. It is able to be stated as:

$$V_{cell} = V_{Nernst} - V_{ohm} - V_{con} - V_{act} \tag{1}$$

Only the gas pressure and flow at the stack's inlet and outlet are taken into account in the cathode channel model, with changes in channel pressure and flow being disregarded. The main function of the cathode flow field model processing is to dynamically simulate the inlet flow, temperature, humidity, pressure, and other gas characteristic parameters as well as the flow of oxygen, nitrogen, and water vapor into the battery at the cathode side. It is considered that all batteries behave similarly because the battery stack is well designed. One stack cathode volume contains the combined cathode volumes of several fuel cells. The oxygen, nitrogen, and water vapor at the cathode are represented by [39] and [40]:

$$\begin{cases} \dfrac{dm_{O_2,ca}}{dt} = W_{O_2,in,ca} - W_{O_2,out,ca} - W_{O_2,react} \\ \dfrac{dm_{N_2,ca}}{dt} = W_{N_2,in,ca} - W_{O_2,out,ca} \\ \dfrac{dm_{v,ca}}{dt} = W_{v,in,ca} - W_{v,out,ca} + W_{v,gen,ca} + W_{v,mem} \end{cases} \tag{2}$$

The mass flow rate of oxygen, nitrogen, and water reaching the stack's cathode is [41]:

$$\begin{cases} W_{O_2,in,ca} = X_{O_2} \times W_{air,in,ca} = X_{O_2} \\ \quad \times \dfrac{W_{in,ca}}{1 - \dfrac{P_{v,in,ca}}{P_{air,in,ca}} \times \dfrac{M_{H_2O}}{M_{air}}} \\ W_{N_2,in,ca} = \left(1 - X_{O_2}\right) \\ \quad \times W_{air,in,ca} = \left(1 - X_{O_2}\right) \times \dfrac{W_{in,ca}}{1 - \dfrac{P_{v,in,ca}}{P_{air,in,ca}} \times \dfrac{M_{H_2O}}{M_{air}}} \\ W_{v,in,ca} = W_{in,ca} - W_{O_2,in,ca} - W_{N_2,in,ca} \end{cases} \tag{3}$$

where the mass flow of dry air entering the cathode is denoted by $W_{air,in,ca}$, $P_{air,in,ca}$ is the air pressure entering the cathode, The oxygen mass percentage in dry air is represented by X_{o2}, and the partial pressure of water vapor entering the cathode is denoted by $P_{v,in,ca}$.

The mass flow rate of dry air and water vapor flowing out of the cathode is:

$$\begin{cases} W_{air,out,ca} = \dfrac{1}{1 + \dfrac{m_{v,ca}}{m_{air,ca}}} W_{out,ca} \\ = \dfrac{1}{1 + \dfrac{P_{v,ca}}{P_{air,ca}} \times \dfrac{M_{H_2O}}{M_{air}}} W_{out,ca} \\ W_{v,out,ca} = W_{out,ca} - W_{O_2,out,ca} - W_{N_2,out,ca} \end{cases} \tag{4}$$

The mass flow rate of the outlet gas can be roughly calculated using the linear nozzle equation due to the cathode cavity's and the cathode outlet pipe's minimal pressure difference [38]:

$$W_{out,ca} = K_{out,ca}\left(P_{ca} - P_{out,ca}\right) \tag{5}$$

where $K_{out,ca}$ are the constant of cathode nozzle and $P_{out,ca}$ are the pressure of exhaust pipeline.

B. EGTAC MODEL

The EGTAC is divided into three parts: compressor assembly, exhaust gas recovery assembly and drive motor. Air enters the compressor from the surrounding environment, and the gas is compressed and delivered to the supply pipeline. The driving motor is responsible for providing necessary power for the air compressor. The gas at the cathode outlet drives the exhaust gas recovery component turbine to rotate through the exhaust gas recovery valve, consequently causing the air compressor to spin quickly. reducing the power demand of the air compressor and saving motor energy.

The real time speed of the air compressor is determined by the driving torque and load torque of the air compressor. Speed characteristic equation of air compressor [39], [42]:

$$\begin{cases} J_{cp}\dfrac{d\omega_{cp}}{dx} = \tau_{cm} - \tau_{cp} \\ \tau_{cm} = \eta_{cm}\dfrac{k_t}{R_{cm}}(v_{cm} - k_v\omega_{cp}) \\ \tau_{cp} = \dfrac{P_{cp}}{\omega_{cp}} \end{cases} \tag{6}$$

where J_{cp} is the linkage inertia between air compressor and motor.

The power consumption of the drive motor is:

$$P_{cp} = \frac{\gamma}{\gamma - 1}\frac{RT_{atm}W_{cp}}{\eta_{cp}}\left(\left(\frac{p_{cp}}{p_{atm}}\right)^{\frac{\gamma-1}{\gamma}} - 1\right) \tag{7}$$

where p_{cp} is the pressure at which the air compressor compresses the gas, η_{cp} is the isentropic efficiency of the air compressor.

The power calculation formula of exhaust gas recovery component is [43] and [44]:

$$P_t = c_{p,ca,out}\eta_{cp}T_{ca,out}\left(\left(\frac{p_{om,out}}{p_{ca,out}}\right)^{1-\frac{1}{\gamma}} - 1\right)\dot{m}_{ca,out} \tag{8}$$

where $c_{p,ca,out}$ are the specific heat capacity of the gas at the cathode outlet.

Combined with the cathode channel model and equation (8), the exhaust gas recovery module model can be defined as follows:

$$P_e = c_{p,ca,out}\eta_t T_{ca,out}\frac{I \cdot N_c}{4F}\left(\pi^{1-\left(\frac{1}{\gamma}\right)} - 1\right) \times \left(M_{O_2}(S-1) + M_{N_2}S\frac{y_{N_2}}{y_{O_2}}\right) \tag{9}$$

C. SUPPLY PIPELINE MODEL

The supply pipeline model describes the connecting pipeline between the air compressor and fuel cell stack, including the connecting pipeline between the intercooler and humidifier. The mass flow at the supply pipeline's outlet is a result of the pressure differential between the cathode flow field and the pipeline outlet [38]:

$$W_{sm,out} = k_{sm,out}\left(p_{sm} - p_{ca}\right) \tag{10}$$

where $k_{sm,out}$ is flow coefficient at the supply pipeline's exit is called out. Before the gas enters the cathode flow field from the air compressor, the temperature in the supply pipeline will change. Determine the gas pressure inside the inlet pipe p_{sm} using the ideal gas state equation [38]:

$$\frac{dp_{sm}}{dt} = \frac{R_a}{V_{sm}}\left(W_{cp}T_{cp,out} - W_{sm,out}T_{sm}\right) \tag{11}$$

where T_{sm} is the temperature of the supply pipeline and R_a is the ideal gas constant.

D. RETURN PIPELINE AND BACK PRESSURE VALVE MODEL

The return pipeline model is used to simulate the pipe change between the discharge of mixed gas from the cathode flow field and the back pressure valve. Similar to the gas supply pipeline model, the dynamic equation of the return pipeline can be expressed as [38]:

$$\frac{dp_{om}}{dt} = \frac{RT_{om}}{V_{om}}\left(W_{ca,out} - W_{om}\right) \tag{12}$$

where p_{om} is the pressure in the flue, T_{om} is the return pipeline temperature, and W_{om} is the air mass flow rate through the return pipeline.

The gas mass flow rate in the return pipeline is:

$$W_{om} = \begin{cases} C_D A_T p_{om}\sqrt{\dfrac{2\gamma}{(\gamma-1)RT_{om}}\left[\left(\dfrac{p_{atm}}{p_{tm}}\right)^{\frac{2}{\gamma}} - \left(\dfrac{p_{atm}}{p_{om}}\right)^{\frac{\gamma-1}{\gamma}}\right]} \\ \dfrac{p_{atm}}{p_{om}} > \left(\dfrac{2}{\gamma+1}\right)^{\frac{\gamma}{\gamma+1}} \\ C_D A_T p_{om}\sqrt{\dfrac{\gamma}{RT_{om}}\left(\dfrac{2}{\gamma+1}\right)^{\frac{\gamma+1}{\gamma-1}}} \\ \dfrac{p_{atm}}{p_{om}} \le \left(\dfrac{2}{\gamma+1}\right)^{\frac{\gamma}{\gamma+1}} \end{cases} \tag{13}$$

where A_T is the opening area of the valve, T_{om} is the gas temperature in the return pipeline, and P_{om} is the gas pressure in the return pipeline.

In this paper, the back pressure valve's opening θ_{om} is controlled to maintain the cathode pressure. Define the back pressure valve opening θ_{om} is:

$$\theta_{om} = \frac{A_T}{\pi r_v^2} \times 100, \theta_{om} \in (0, 100) \tag{14}$$

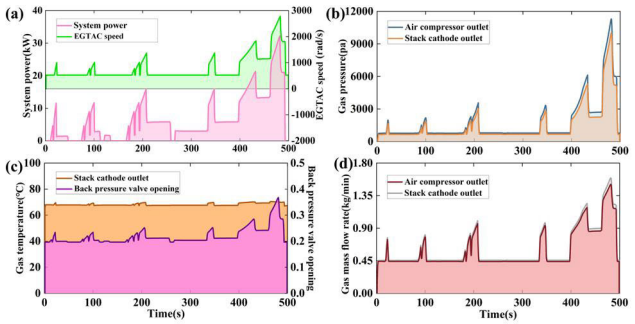

FIGURE 2. Simulation results of cathode exhaust and EGTAC in fuel cell system (a) system load power and EGTAC speed; (b) Outlet gas pressure; (c) Outlet gas temperature and back pressure valve opening; (d) Outlet gas pressure mass flow rate.

E. FUEL CELL SYSTEM POWER AND EFFICIENCY

A fuel cell stack consists of multiple individual cells that are interconnected in a series configuration. The stack power is:

$$P_{st} = n_{st} V_{cell} I_{st} \tag{15}$$

A vehicle fuel cell system comprises an air supply system, a hydrogen supply system, a thermal management system, and an electric stack. The EGTAC is the component that consumes the most power in the fuel cell system. Parasitic elements such as the hydrogen circulation pump, water pump, and cooling fan also contribute to power consumption. However, when compared to the power consumption of the EGTAC, their impact on the output power of the fuel cell system is minimal and can be disregarded. Hence, this study just focuses on the power consumption of the EGTAC, disregarding the impact of other parasitic components. The system output power is determined by subtracting the power consumption of parasitic components from the effective output power of the stack [45]:

$$P = P_{st} - P_{cp} \tag{16}$$

where P_{CP} is the power of parasitic components. The electric efficiency of fuel cell system is [46]:

$$\eta_{fc} = \frac{P}{P_{st}} \tag{17}$$

The main parameters in the model of the of PEMFC satck model and air supply system are shown in Table 1.

F. MODEL SIMULATION RESULTS

Based on the aforementioned mathematical model, this study employs Amesim software to construct a simulation model of a fuel cell system that includes EGTAC. The system undergoes 500s variable load power simulation, and simulation results are displayed in Figure 2. Figure 2(a)'s pink curve represents the applied load power of fuel cell system, while the simulation outcome of the EGTAC speed is depicted by the green curve. The alteration of the EGTAC's velocity is essentially in accord with the modification of load power in the fuel cell system. The reason is that an elevation in the load power necessitates an increase in gas supply for the system, and correspondingly, the EGTAC must generate a higher gas flow to meet this requirement. As a result, the velocity is adjusted accordingly. The findings of the simulation for the gas pressure at the EGTAC's outlet and the stack's cathode are exhibited in Figure 2(b). The gas pressure at both the EGTAC's outlet and the stack's cathode is subject to change in line with variations in load power. This is done to satisfy the cathode's requirement for an adequate supply of oxygen. The simulation results for the opening of back pressure valve and the gas temperature at the cathode outlet of the stack are presented in Figure 2(c). By controlling the gas flow's resistance at both the cathode outlet and exhaust pipe, the valve's opening will increase in proportion to the load power rise. The back pressure valve's opening can stabilize the gas flow and pressure, yet the temperature at the cathode outlet of the stack remains stable at approximately 67°C; Figure 2(d) displays the simulation findings for the gas mass flow rate at the cathode outlet of the EGTAC and stack. The gas mass flow rate at the outlet of the EGTAC will change correspondingly with the load power variation as the outlet gas pressure changes. Therefore, the cathode outlet pressure and fuel cell mass flow rate have been chosen as parameters for estimating

TABLE 1. Main parameters of PEMFC satck model and air supply system model.

Parameter	Unit	Valve
Stack operating temperature T_{st}	K	352
Number of single cells n_{st}		382
Faraday constant F		96485
Reaction area A_{act}	m^2	0.02
Designed power of stack P_{fc}	kW	115
Volume of cathode flow field V_{ca}	m^3	0.01
Nozzle constant of cathode $K_{ca,out}$	$kg/(s{\cdot}Pa)$	2.1776×10^{-6}
Molar mass of oxygen M_{O2}	kg/mol	0.032
Molar mass of nitrogen M_{N2}	kg/mol	0.028
Molar mass of water M_{H2O}	kg/mol	0.018
Molar mass of dry air M_{air}	kg/mol	0.029
Gas constant of air R_a	$J/(kg{\cdot}K)$	298.6
adiabatic exponent of air γ		1.4
Specific Heat Capacity of Air C_p	$J/kg{\cdot}K$	1004.88
Motor torque sensitivity constant k_t	$N{\cdot}m/A$	0.0153
Motor back EMF constant k_v	$V/(rad/sec)$	0.0153
Armature resistance R_{cm}	Ω	0.9
Air compressor inlet air temperature T_{atm}	K	298.15
Air compressor inlet air pressure P_{atm}	Pa	101,325
Flow coefficient of the supply manifold outlet $k_{sm,out}$		3.629×10^{-6}
Volume of the supply manifold V_{sm}	m^3	0.02
The flow coefficient of the reflux pipeline C_D		0.0124
Volume of the return pipeline V_{om}	m^3	1.52×10^{-3}
Back pressure valve radius r_v	m	0.0228

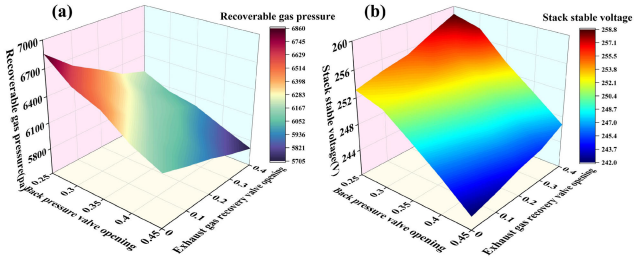

FIGURE 3. Effect of valve opening on (a) recoverable gas pressure; (b) Stable voltage of stack.

research and exhaust characteristics which enables reflection and analysis of the performance and working efficiency of the EGTAC and fuel cell system under diverse load power.

III. CONTROL PARAMETER IMPACT ANALYSIS AND ESTIMATION OF CATHODE EXHAUST CHARACTERISTICS

A. EFFECT OF VALVE OPENING ON EXHAUST ENERGY AND FUEL CELL PERFORMANCE

To study the influence of the back pressure valve and exhaust gas recovery valve opening on the operation of the stack and the EGTAC, this paper selects the working condition of the fuel cell system loaded at 60% of the rated power for the study, and sets the back pressure valve opening to 0.25, 0.3, 0.35, 0.4 and 0.45 in order, and the exhaust gas recovery valve opening to 0, 0.1, 0.2, 0.3, 0.4, the recoverable exhaust gas of the EGTAC and the stable voltage of the stack under different opening of the two valves are shown in Figure 3: Figure 3.(a) is the EGTAC can be recovered gas pressure with the change of these two valve openings, when the exhaust gas recovery valve opening is kept constant at 0, with the backpressure valve opening is reduced from 0.45 to 0.25, the EGTAC can be recovered gas pressure increases from 6102.3Pa to 6856.7Pa. When the 0.45 backpressure valve opening remains constant, the recoverable gas pressure of the EGTAC decreases from 6102.3 Pa to 5704.5 Pa as the exhaust gas recovery valve opening increases from 0 to 0.4; Figure3(b) shows the variation of the fuel cell stack's stabilized voltage with the change of these two valve openings When the backpressure valve opening is kept constant at 0.45, the stable voltage of the stack increases from 242.1V to 246.8V as the exhaust gas recirculation valve opening increases from 0 to 0.4. When the backpressure valve opening is kept constant at 0.25, the stable voltage of the stack increases from 242.1V to 253.2V as the exhaust gas recirculation valve opening increases from 0 to 0.4. This is because when the back pressure valve's opening is reduced, the resistance of exhaust gas emission is increased, and the gas pressure in the stack's cathode outlet, i.e. the exhaust pipeline, is increased which allows the EGTAC to recover the energy in the flue gas more effectively, increasing the amount of air entering the stack and improving stack performance. Similarly, if the exhaust gas recirculation valve opening is increased, the EGTAC will start to recirculate the exhaust gas, and the gas

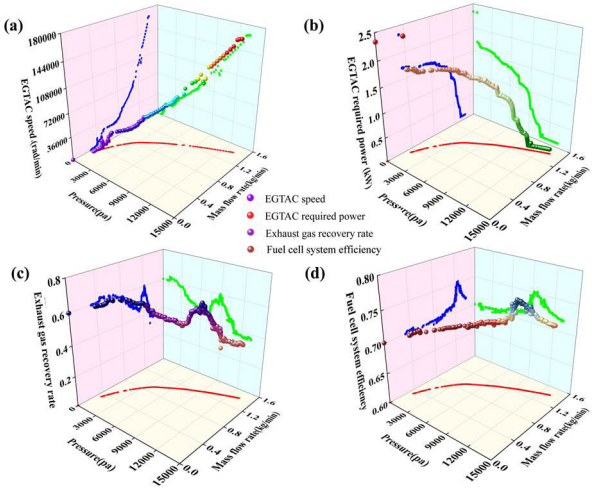

FIGURE 4. Effect of exhaust gas energy recovered by the EGTAC on (a) EGTAC speed; (b) Required power of EGTAC; (c) Exhaust gas recovery rate; (d) fuel cell system efficiency.

at the cathode outlet of the stack will decrease, and then the air entering the stack will increase, and the performance of the stack will also improve. However, if the opening of the backpressure valve is set too small for a long time, the cathode reaction gas will not be discharged, which can easily damage the internal structure of the stack.

B. EFFECT OF RECOVERED EXHAUST GAS ENERGY ON FUEL CELL SYSTEM PERFORMANCE

To further investigate the specific effect of exhaust gas energy recovered by the EGTAC on the performance of the EGTAC and fuel cell system, this paper chooses to increase the gas pressure recovered by the EGTAC from 655.52 Pa to 13233.89 Pa, and the mass flow rate of recovered gas from 0.32356 kg/min to 1.4179 kg/min. The performance of the EGTAC and the stack under the change of exhaust gas energy recovered by the EGTAC is shown in Figure 4: Figure 4(a) shows that with the increase of extracted energy from the exhaust gas by the EGTAC, the EGTAC speed is almost linear with increasing speed; Figure 4(b) demonstrates that when the energy of the exhaust gas that the EGTAC recovers rises, the power required by the EGTAC gradually decreases; at the beginning of exhaust gas recovery by the EGTAC, that is, when the gas pressure is less than 8000 Pa, the EGTAC still needs to be driven by the engine, and the power required by the EGTAC decreases relatively slowly, when the energy of the exhaust gas increases, that is, when the gas pressure reaches 9000 Pa, the power required by the EGTAC decreases relatively rapidly, but when the energy of the exhaust gas is sufficiently high, that is, when the gas pressure is greater than 12,000 Pa, the power required by the EGTAC does not continue to decrease; Define the calculation formula of the energy recovery efficiency of the exhaust gas of the EGTAC as: $\eta_e = W_1/W_0$. Where W_1 is the mass flow at the outlet of the exhaust gas recovery comp,

W_0 is the mass flow at the EGTAC exhaust gas recovery component's input. Figure 4(c) shows that the efficiency of EGTAC gas recovery gradually decreases as the energy of EGTAC gas recovery increases. When the exhaust pressure reaches 7769.34 Pa, the efficiency of the EGTAC exhaust gas recovery increases and continues to decrease after reaching the local peak when the exhaust pressure reaches 8949.98 Pa; Figure 4(d) shows that the efficiency of the fuel cell system slowly increases from 70.1% with the increase of the energy recovered from the exhaust gas by the EGTAC. When the exhaust pressure reaches 7713.67 Pa, the efficiency of the fuel cell system increases rapidly reaching about 75.3%, and starts to decrease after reaching the maximum value of the fuel cell system when the exhaust pressure reaches 9127.46 Pa. This is because as the recovered exhaust energy increases, it can be used to provide more power, drive the EGTAC to rotate faster, reduce the power required by the EGTAC, and thus improve the fuel cell system's efficiency. However, the capacity of the EGTAC to recover exhaust gas is limited, so the efficiency of exhaust gas recovery is reduced. When the energy recovered from the exhaust gas is sufficient, the exhaust gas recovery system is saturated and the power consumption of the EGTAC has reached a stable state, at which time more exhaust gas energy cannot be effectively used, and the efficiency of the fuel cell has decreased, but it is still higher than the efficiency of the system without exhaust gas recovery.

C. OBSERVATION OF GAS STATE AT CATHODE OUTLET OF FUEL CELL

Owing to the fuel cell's broad working range, variations in mass flow and gas pressure at the stack's cathode outlet will result in variations in the exhaust gas recirculation system's output, and it is easy to render the exhaust gas recirculation system ineffective. Based on the above, the exhaust gas supply directly affects the output of the EGTAC. If the oxygen supply is insufficient, the energy generated by the exhaust gas cannot meet the power demand of the EGTAC; if the exhaust gas supply is too high, the parasitic power of the exhaust gas recovery component increases, affecting the efficiency of the exhaust gas recovery. Exhaust energy control refers to the control of gas pressure and mass flow in the channel at the cathode outlet side of the stack. However, it is challenging to measure the pressure at the cathode outlet of the stack $p_{ca,out}$. Therefore, the soft measurement method is adopted, i.e. Realtime pressure estimates are intended to be provided by the state observer, and the mass flow is estimated according to the cathode pressure estimated in real time.

Based on the model established in section II, the model of the fuel cell air supply system can be written as a nonlinear state space equation, as shown in the formula:

$$\begin{cases} \dot{x} = g(x) \cdot u + f(x) \\ y = Cx \end{cases} \tag{18}$$

where, state $x \in R^6$, $x = [m_{o2,ca}\ m_{N2,ca}\ \omega_{cp}\ W_{sm,out}\ p_{sm}\ p_{om}]^T$, model input $u \in R^2$, $u = [\theta_e\ \theta_{rm}]^T$, model input $y \in R^2$, $y = [\omega_{cp}\ p_{sm}]^T$, can be measured by sensor. C is the measurement matrix. Matrices $f(x)$ and $g(x)$ can be written as (19) and (20), as shown at the bottom of the next page.

Regarding the state $p_{ca,out}$ to be observed as a new state x_7, the equation of state x_6 can be rewritten as:

$$\begin{cases} \dot{x}_6 = k_{sm}\dfrac{V_{om}}{R_a}x_7 - k_{sm}\dfrac{V_{cm}}{R_a}x_6 + g\,(x_6)\cdot u_2 \\ \dot{x}_7 = \mu(t) \end{cases} \tag{21}$$

where, $g(x_6) = k_{ca,out}R_aT_{om}W_{om}x_6/V_{om}$, Due to the complexity of the dynamic characteristics of $p_{ca,out}$, its variation is temporarily represented by $\mu(t)$, and the observer is designed as:

$$\begin{cases} \vec{x}_6 = k_{sm}\dfrac{V_{om}}{R_a}\vec{x}_7 - k_{sm}\dfrac{V_{cm}}{R_a}\vec{x}_6 + \alpha_1\left(x_6 - \vec{x}_6\right) \\ \vec{x}_7 = \alpha_2\left(x_6 - \vec{x}_6\right) \end{cases} \tag{22}$$

where, $\vec{x}_6$ and $\vec{x}_7$ are the estimated values of states x_6 and x_7 respectively, α_1 and α_2 is the parameter to be determined. Through Simulink simulation, the values of α_1 and α_2 are determined to be 50 and 450. Therefore, we can get the estimated values of the observed $p_{ca,out}$ and $W_{ca,out}$:

$$\begin{cases} \vec{p}_{ca,out} = \vec{x}_7 \\ \vec{W}_{ca,out} = \chi_{v,in}k_{sm}\left(x_6 - \vec{p}_{ca,out}\right)/\dfrac{nM_vI_{st}}{4F} \end{cases} \tag{23}$$

To verify the accuracy of the state observer, simulation tests were performed on the Simulink platform. Figures 5 to 7 show the comparison results of the estimation of the cathode outlet pressure and mass flow of the fuel cell system in various load scenarios. The estimation results of the gas characteristics at the cathode outlet of the stack under high load power are shown in Figure 5: Figure 5(a) shows the applied load power, and Figure 5(b) and Figure 5(c) show the observation and comparison results of the cathode outlet pressure and mass flow rate of the fuel cell under this load, which can accurately estimate the exhaust gas characteristics. From the local enlarged view, it is more obvious that the designed observer can better follow the measured values of the sensor, Figure 5(d) and Figure 5(e) show the estimation error of pressure and mass flow rate under this load. The maximum error rate of pressure estimation is less than 13.84% and the maximum error rate of mass flow estimation is less than 12.10%.

The estimation results of the gas characteristics at the cathode outlet of the stack under medium load power are shown in Figure 6: Figure 6(a) shows the applied load power, and Figure 6(b) and Figure 6(c) show the observation and comparison results of the cathode outlet pressure and mass flow rate of the fuel cell under this load. It is more obvious that the designed observer can better follow the measured value of the sensor from the local enlarged view, and Figure 6(d) and Figure 6(e) show the estimation error of pressure and mass flow rate under this load. The maximum error rate of pressure estimation is less than 13.23%, and the maximum error rate of mass flow estimation is less than 11.60%.

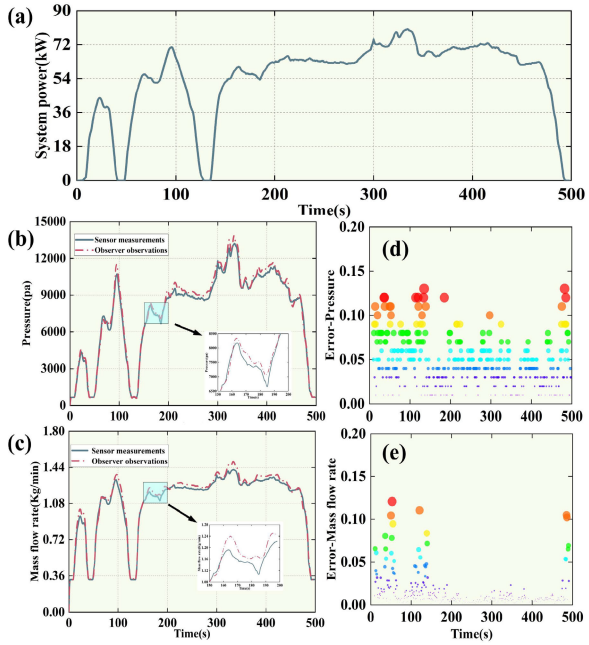

FIGURE 5. Comparison of gas state sensor and observer at cathode outlet of stack under high load power.

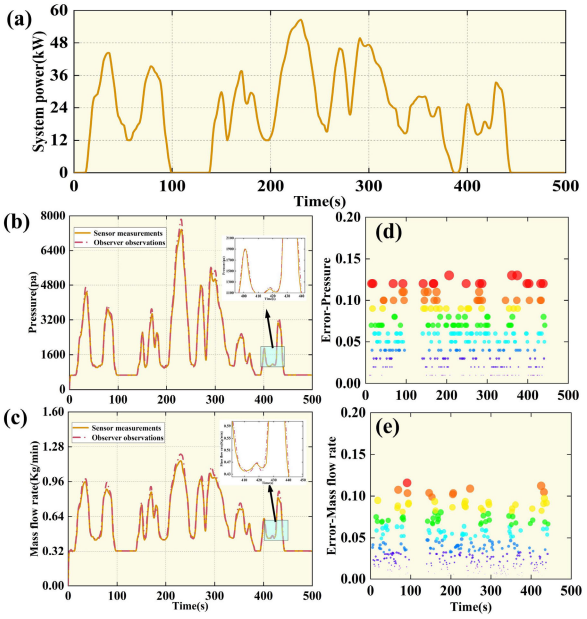

FIGURE 6. Comparison of gas state sensor and observer at cathode outlet of stack under medium load power.

The estimation results of the gas characteristics at the cathode outlet of the stack under low load power are shown in Figure 7: Figure 7(a) shows the applied load power, and Figure 7(b) and Figure 7(c) show the observation and comparison results of the cathode outlet pressure and mass flow rate of the fuel cell under this load. It is more obvious that the designed observer can better follow the measured value of the sensor from the local enlarged view, Figure 7(d) and Figure 7(e) show the estimation error of pressure and mass flow rate under this load. The maximum error rate of pressure estimation is less than 11.63%, and the maximum error rate of mass flow rate estimation is less than 10.89%. Therefore, the designed observer can track the gas pressure at the cathode outlet well and the estimation error is within the acceptable range.

IV. EGTAC ENERGY RECOVERY OPTIMIZATION INTELLIGENT CONTROL METHOD

A. CONTROL STRUCTURE OF THE EGTAC BASED ON DDPG ALGORITHM

This paper proposes an intelligent control architecture of the EGTAC founded on the deep deterministic policy gradient (DDPG), as shown in Figure 8(a). The framework takes the PEM fuel cell system as the environment and the DDPG algorithm as the intelligent agent. The goal is to improve the

$$f(x)=\begin{bmatrix} \frac{k_{ca}M_{O_2}x_1}{M_{O_2}x_1+M_{N_2}x_2+M_v}\left(x_6-p_{ca,out}\right)+k_{sm}\chi_{O_2}\left(x_5-p_{ca,out}\right) \\ \frac{k_{ca}M_{N_2}x_2}{M_{O_2}x_1+M_{N_2}x_2+M_v}\left(x_6-p_{ca,out}\right)+k_{sm}\chi_{N_2}\left(x_5-p_{ca,out}\right) \\ \frac{\eta_{cm}k_tk_v}{J_{cp}R_{cm}}x_3-\frac{C_pT_{atm}}{J_{cp}\eta_{cp}}x_3^{-1}\left[\left(\frac{x_5}{p_{atm}}\right)^{\frac{\gamma-1}{r}}-1\right]W_{cp,out} \\ k_{sm}\frac{x_5}{x_4}\left(p_{ca,out}-x_5\right)+\frac{\gamma R_a}{V_{sm}}T_{atm}W_{cp,out}\left[1+\frac{1}{\eta_{cp}}\left(\frac{x_5}{p_{atm}}\right)^{\frac{\gamma-1}{r}}\right] \\ W_{cp,out}-k_{sm}\left(x_5-p_{ca,out}\right) \\ k_{sm}\frac{V_{cm}}{R_a}\left(p_{ca,out}-x_6\right) \end{bmatrix} \tag{19}$$

$$g(x)=\begin{bmatrix} 0 & 0 \\ 0 & 0 \\ \frac{\eta_{cm}k_t}{J_{cp}R_{cm}} & 0 \\ 0 & 0 \\ 0 & 0 \\ 0 & -k_{ca}\frac{R_aT_{om}}{V_{rm}}W_{om,out} \end{bmatrix} \tag{20}$$

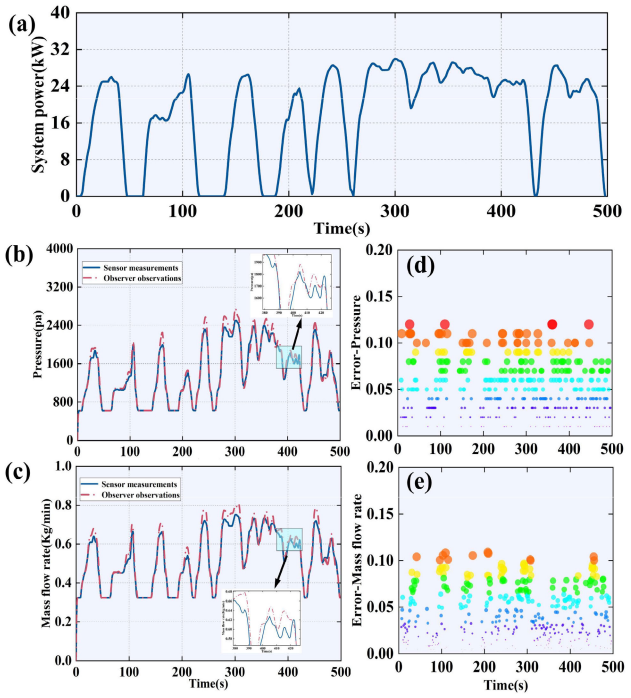

FIGURE 7. Comparison of gas state sensor and observer at cathode outlet of stack under low load power.

fuel cell system's efficiency while improving the efficiency of the EGTAC exhaust gas recovery. The algorithm flow of DDPG is shown in Table 2.

In DDPG algorithm, state and action are important components of learning.

The state quantity s_t is expressed as:

$$s_t = \left\{P_{cp}, W_{rm}, p_{rm}, p_{ca,out}, W_{ca,out}\right\} \tag{24}$$

The energy of exhaust gas entering the EGTAC is managed by modifying the exhaust gas recovery valve's and back pressure valve's opening, so the action a_t is:

$$a_t = \{\theta_{BPV}, \theta_{EGR}\} \tag{25}$$

The reward plays the role of guiding the agent to learn and optimize strategies. The reward r is set as:

$$R = \left\{k_1\eta_e^2 + k_2\eta_{fc}^2\right\} \tag{26}$$

where k_1 and k_2 are weight coefficients.

B. DDPG ALGORITHM TRAINING AND TRAINING RESULTS ANALYSIS

DDPG is an optimization algorithm that based on a deterministic strategy. The algorithm's training process involves sending the state variables of the fuel cell system (such as the power consumption of the driving motor, the gas pressure through the Return pipeline, the gas mass flow through the Return pipeline, the gas pressure at the cathode outlet, and the gas mass flow at the cathode outlet) to the DDPG training environment to train the agent. The Actor network determines

TABLE 2. DDPG algorithm flow.

DDPG algorithm flow
Input: policy current network parameters θ^{μ}, Policy target network parameters $\theta^{\mu'}$, Evaluate current network parameters θ^{Q}. Evaluation target network parameters$\theta^{Q'}$, attenuation factor γ, Soft renewal coefficient τ, The number of empirical playback samples n, the target network parameter update frequency f, the number of iteration rounds M, the number of single round iterations T, and the random process N
Output: optimal policy current network parameters θ^{μ} and evaluate current network parametersθ^{Q}
1. random initializationθ^{μ}, θ^{Q}, Concurrent order $\theta^{\mu'}=\theta^{\mu}$, $\theta^{Q'}=\theta^{Q}$. Initialize experience playback pool P
2. For rounds=1 : M do
Obtain initial state S_1
For t=1 : T do
a) Based on the current network of the policy, enter the state St to get the action $A_t=\mu(S_t)+N_t$
b) Execute action A_t to get new status S_{t+1} and reward R_t
c) Store (S_t, R_t, A_t, S_{t+1}) in P
d) Let $S_t=S_{t+1}$
e) Randomly sample n samples (S_i, R_i, A_i, S_{i+1}), i=1, 2, ..., n, and calculate the current target Q value y_i $y_i = R_i + \gamma Q'(S_{i+1}, \mu'(S_{i+1}), \theta^{Q'})$
f) Based on the mean square loss function, $L = \frac{1}{n}\sum_{i=1}^{n}(y_i - Q(S_i, A_i, \theta^{Q}))^2$ the parameters of the current network are updated by gradient back propagationθ^{Q}
g) Based on the loss function, $J(\theta^{\mu}) = -\frac{1}{n}\sum_{i=1}^{n}(Q(S_i, A_i, \theta^{Q}))$ the parameters of the current network are updated by gradient back propagation strategy θ^{μ}
h) When M%f=1, update the evaluation target network and strategy target network parameters:
$\theta^{Q'} = \tau\theta^{Q} + (1-\tau)\theta^{Q'}$
$\theta^{\mu'} = \tau\theta^{\mu} + (1-\tau)\theta^{\mu'}$
end for
end for

the action, (i.e. the opening of the back pressure valve and the exhaust gas recovery valve), based on the current state. It then feeds the current action and state into the Critic network to calculate the Q value. Finally, the Actor network parameters are updated using gradient ascent. then, the action value is assigned to each component as the provided value, and then, the matching reward and penalty value is acquired through the utilization of the specified reward and penalty function. Simultaneously, the subsequent state is derived depending on the current state. The Critic network updates its parameters using gradient descent between the current action and state, and the future action and state. This process is described by the following formula:

$$L\left(\boldsymbol{\theta}^{Q}\right) = E\left[\left(r + \gamma Q_T\left(\boldsymbol{s}', \boldsymbol{a}' \mid \boldsymbol{\theta}_T^{Q}\right) - Q\left(\boldsymbol{s}, \boldsymbol{a} \mid \boldsymbol{\theta}^{Q}\right)\right)^2\right] \tag{27}$$

$$\nabla_{\boldsymbol{\theta}^{\mu}} Q \approx E\left[\nabla_{\boldsymbol{a}} Q\left(\boldsymbol{s}, \boldsymbol{a} \mid \boldsymbol{\theta}^{Q}\right)\Big|_{\boldsymbol{a}=\mu(\boldsymbol{s})} \cdot \nabla_{\theta^{\mu}} \mu\left(\boldsymbol{s} \mid \boldsymbol{\theta}^{\mu}\right)\right] \tag{28}$$

TABLE 3. Units for magnetic properties.

Parameter	Parameter value
Training rounds episodes	1000
Memory pool capacity N	10000
Minimum sample set sample	36
Nnumber n	
Actor learning rate	0.002
Critic learning rate	0.0012
Discount rate	0.99

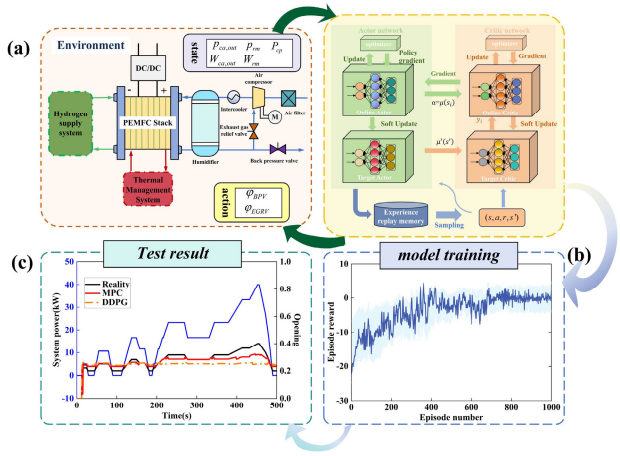

FIGURE 8. EGTAC energy recovery control architecture based on DDPG algorithm.

where $L(\theta^Q)$ is the average loss function; θ^μ and θ^Q is the parameter of strategy network Actor and evaluation network Critic respectively; θ_T^Q is the parameter of target Critic; $\gamma \in [0, 1]$ is the discount factor; $Q(s, a|\ \theta^Q)$ is the Q value of the current state-action pair; $Q_T(s', a'|\ \theta_T^Q)$ is the Q value of the next time state-action pair; $\mu(s, a|\ \theta^\mu)$ is the policy output from the Actor network, where the target network structure is the same as the current network structure. When the average loss function converges, the algorithm is trained. At this time, the Actor network is the optimal strategy, which can realize the real-time control of the energy recovery of the EGTAC.

Before the training is officially started, it is necessary to build a connection network and explain the training parameters of the agent agent. The training parameter values of DDPG are shown in Table 3.

Figure 8(b) depicts the round awards and average rewards of the EGTAC exhaust gas energy recovery control method training. The algorithm takes 4.5 hours to train 1000 rounds. The single reward tends to converge during 780 training rounds. The round reward and the average reward are gradually improved during continuous training, which shows that the algorithm gradually improves the reward performance in the learning process. The training results show that the parameter setting and network structure of the DDPG algorithm are reasonable.

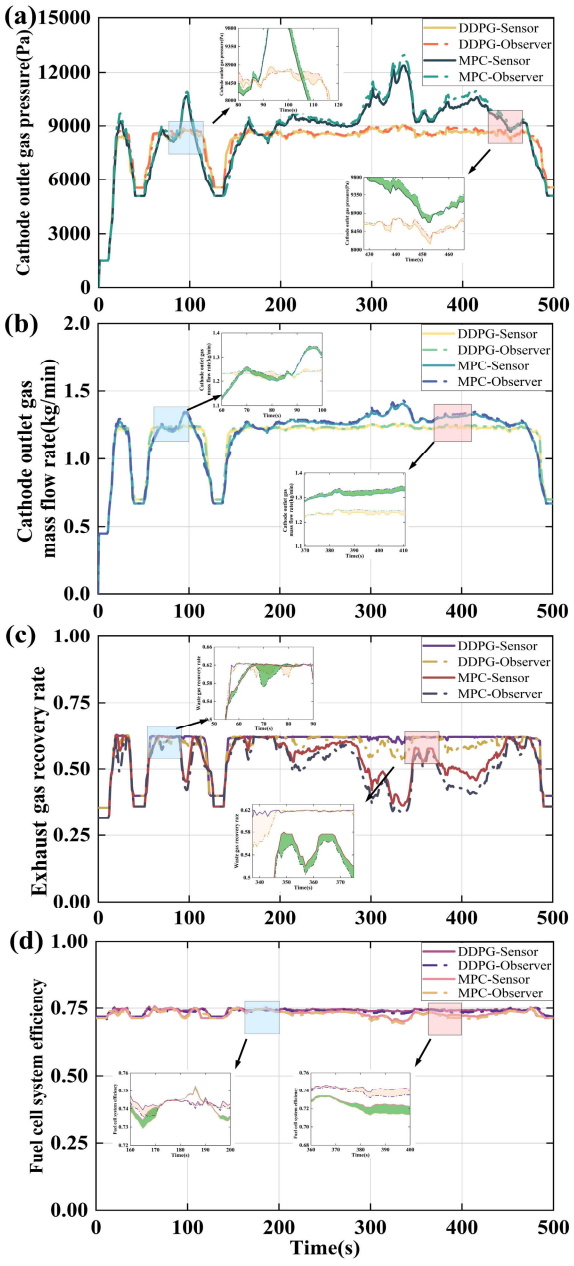

FIGURE 9. Control results under high-power condition (a) cathode outlet gas pressure; (b) Gas mass flow rate at cathode outlet; (c) EGTAC exhaust gas recovery rate; (d) Fuel cell system efficiency.

C. CONTROL METHOD TEST RESULTS

In this work, the variable load data of the fuel cell system is selected as the test condition, as shown in Figure 8(c). Compare the backpressure valve's opening with the MPC control. When the fuel cell system increases and decreases the load, the MPC cannot control the back pressure valve's opening well, and instability will occur; however, under the control of the DDPG, the opening of the back pressure valve can be accurately and stably controlled in the target range, which has good robustness.

D. RESULT ANALYSIS

The control outcomes of two different control algorithms based on sensor and observer under high power load conditions for exhaust gas pressure and gas mass flow rate entering the EGTAC are displayed in Figures 9(a) and 9(b). With the modification of load power, the gas pressure governed by the sensor and observer under the DDPG essentially maintains stability around 8540.43 Pa, the gas pressure observed by the observer is higher than that measured by the sensor in most control times within 500s, and the maximum error between the two is less than 296.53 Pa. The gas mass rate remains essentially stable at around 1.22 kg/min, the gas mass flow rate observed by the observer is also higher than that measured by the sensor in most control times within 500s, and the maximum error between the two methods is less than 0.09 kg/min. Nevertheless, when subjected to the MPC, the exhaust gas pressure and mass flow rate exhibit significant fluctuations. However, when comparing the results obtained from the control based on sensor and observer under the MPC, the two methods' error is also small.

The results of controlling and optimizing the EGTAC exhaust gas recovery rate and the fuel cell system efficiency are presented in Figures 9(c) and 9(d) respectively. As the load power changes, the sensor-based EGTAC exhaust gas recovery rate remains stable at over 60.1% under the DDPG, which is 21.5% higher than that of the MPC. However, the optimization effect of the observer-based EGTAC exhaust gas recovery rate is worse than that of the sensor-based EGTAC when controlled by the DDPG, the maximum difference is less than 6.5%. Furthermore, the efficiency of the sensor-based fuel cell system when controlled by the DDPG remains stable at over 74.2%, which is 3.6% higher than that seen with the MPC. The optimization efficiency of fuel cell system based on observer controlled by the DDPG is also inferior to that of the optimization efficiency fuel cell system based on sensor. Nevertheless, the maximum difference is less than 2.0%.

Under the condition of high power load, the gas pressure and gas mass flow rate observed by the observer are higher than those measured by the sensor under the same algorithm control. The difference arises from the observer's mistake in monitoring the exhaust gas characteristics. Consequently, the optimization of the EGTAC exhaust gas recovery rate and fuel cell system efficiency, when controlled by the DDPG based on the observer, is inferior to that based on the sensor. However, the difference is small, therefore indicating that the proposed sensorless control method is really efficient in the condition of high power load.

The control outcomes of two different control algorithms based on sensor and observer under medium power load conditions for exhaust gas pressure and gas mass flow rate entering the EGTAC are displayed in Figures 10(a) and 10(b). With the modification of load power, the gas pressure governed by the sensor and observer under the DDPG essentially maintains stability around 8528.81 Pa, different from the case under high power load condition, the gas

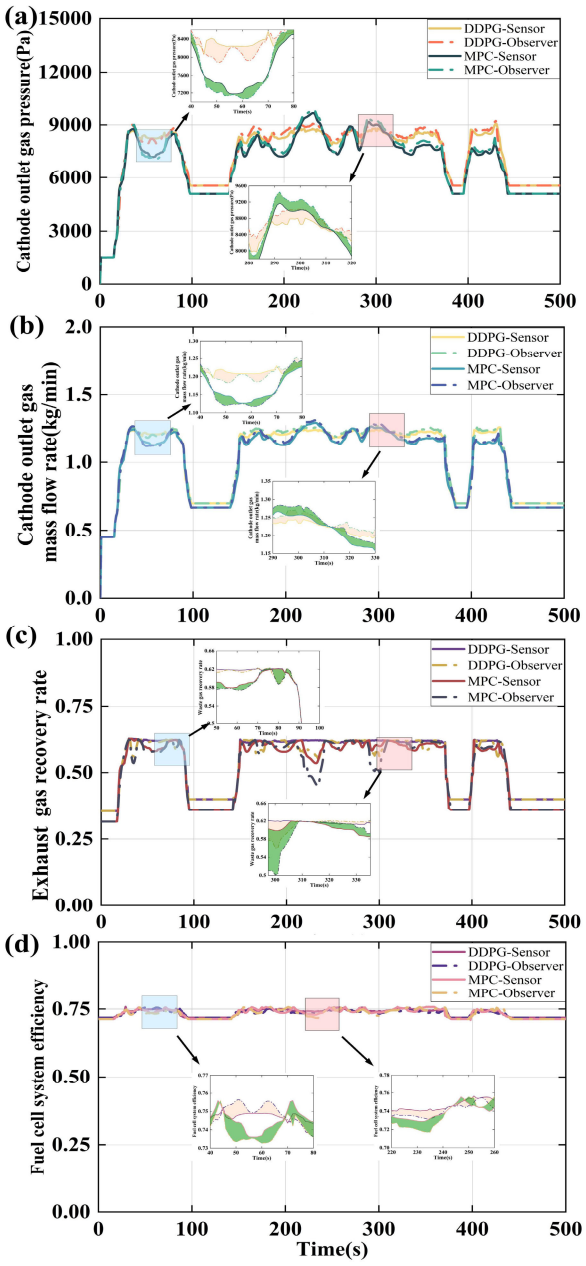

FIGURE 10. Control results under medium power condition (a) cathode outlet gas pressure; (b) Gas mass flow rate at cathode outlet; (c) EGTAC exhaust gas recovery rate; (d) Fuel cell system efficiency.

pressure observed by the observer and that measured by the sensor are high and low within 500s, but the maximum error between the two is less than 322.90 Pa. The gas mass rate remains essentially stable at around 1.22 kg/min, the gas mass flow rate observed by the observer and that measured by the sensor are also high and low within 500s, but the maximum error between the two is less than 0.15 kg/min. Similar to the high power load condition, the fluctuation of exhaust gas pressure and mass flow rate under the control of MPC is higher than that of DDPG. However, compared with the control results obtained using sensors and observers, the two methods' error is also low. The

results of controlling and optimizing the EGTAC exhaust gas recovery rate and the fuel cell system efficiency are presented in Figures 10(c) and 10(d) respectively. As the load power changes, the sensor-based EGTAC exhaust gas recovery rate remains stable at over 61.08% under the DDPG, which is 13.5% higher than that of the MPC, the optimization of the observer-based EGTAC exhaust gas recovery rate, under the DDPG, is generally inferior to that of sensor-based optimization. However, there are certain periods, particularly when there is a sudden change in gas pressure change rate, where the observer-based optimization outperforms the sensor-based optimization. The maximum difference is less than 5.8%. Furthermore, the efficiency of the sensor-based fuel cell system under the DDPG remains stable at over 74.3%, which is 2.8% higher than that seen with the MPC. Similar to the results of exhaust gas recovery rate, the efficiency optimization effect of observer-based fuel cell system under the DDPG is worse than that of sensor-based optimization in most periods, but better than that of sensor based optimization in some periods, and the maximum difference is less than 1.4%.

Under the medium power load condition, the gas pressure and gas mass flow rate observed by the observer may either exceed or fall below the values measured by the sensor, under the same algorithm. The reason for this result is that the applied medium power load changes more frequently, and the estimation of cathode gas characteristics of fuel cell system has deviation. Nevertheless, the fuel cell's cathode exhaust is reduced during medium power load conditions, resulting in a smaller error in estimating gas characteristics compared to high power load conditions. Consequently, the optimization of the EGTAC exhaust gas recovery rate and fuel cell system efficiency based on observer under the same algorithm control is sometimes better than that based on sensor, and sometimes worse than that based on sensor, but the difference is smaller than that under high power load condition. Hence, the proposed sensorless control method is efficient in the condition of medium power load. Because the exhaust gas energy of the system is less under the low power load condition, this paper does not consider its control. Furthermore, under high power load conditions and medium power load conditions, compared with the electrical efficiency results of the fuel cell system obtained by controlling the air supply system to optimize the response characteristics and power density of the fuel cell in literature [47], [48], [49], the efficiency of the fuel cell system optimized based on the cathode exhaust gas energy recovery control in this study is at a reasonable level. According to the study of the control optimization findings presented above, the sensorless estimating method proposed can substitute the sensor function and significantly enhance the efficiency of exhaust energy recovery and fuel cell system.

V. CONCLUSION

This study examines how the recovery of energy from the EGTAC affects fuel cell system performance. Additionally, a method for estimating the exhaust gas characteristics at the cathode outlet of the stack is proposed, and a sensorless control method for exhaust gas energy recovery, utilizing reinforcement learning algorithms, is designed to optimize the performance of both the EGTAC and the fuel cell system. From these workings, conclusions are drawn.

(1) When the back pressure valve's opening decreases during loading of the PEMFC, it causes an increase in gas flow and pressure entering the EGTAC due to the rise in cathode exhaust gas from the stack which reduces the power requirement of the EGTAC. With an increase in exhaust pressure from 7713.67 Pa to 9127.46 Pa, the effectiveness of fuel cell system improves by 3.2%. However, the energy required by the EGTAC does not invariably diminish with higher exhaust gas energy, as the EGTAC has constraints in recuperating exhaust gas, leading to a decline in fuel cell system efficiency after it reaches the peak.

(2) This paper proposes a method to estimate the exhaust characteristics of fuel cell systems by estimating the pressure of the cathode outlet gas of the stack using a state observer and calculating the mass flow rate based on it. The simulation results of 500s under three different load powers show that the maximum error rates of pressure and mass flow rate estimation are less than 13.84% and 12.1%, respectively, and the estimation error rates are less than 10% for 80% of the simulation time. This method achieves accurate tracking of the characteristics of the cathode outlet gas.

(3) The sensorless control technique presented in this paper aims to optimize the efficiency of the EGTAC and fuel cell system. It possesses excellent decision making capabilities and strong learning ability. The study demonstrates that the exhaust gas recovery rate of the EGTAC increased by 19.1% and 12.7%, while the fuel cell system's efficiency improved by 3.7% and 2.3% under high and medium loads, respectively, and the maximum difference is less than 6.5% compared with the control effect with sensors, which indicates that the suggested observer-based control approach for recovering energy from fuel cell exhaust can estimate gas characteristics accurately at the cathode outlet, offering guidance for controlling the exhaust gas recovery process. Consequently, the stability of the EGTAC operation is ensured, and the fuel cell system can achieve efficient output performance.

REFERENCES

[1] D. Hu, W. Hou, C. Xiang, D. Lu, Q. Yang, J. Li, and J. Wang, "Waste heat utilization performance verification of heat exchanger only thermal management system for fuel cell vehicle," *J. Cleaner Prod.*, vol. 428, Nov. 2023, Art. no. 139479, doi: 10.1016/j.jclepro.2023.139479.

[2] D. Hu, Y. Wang, J. Li, J. Wang, and Q. Yang, "Energy saving control of waste heat utilization subsystem for fuel cell vehicle," *IEEE Trans. Transport. Electrific.*, early access, Aug. 15, 2024, doi: 10.1109/TTE.2023.3304844.

[3] J. Li and T. Yu, "Intelligent controller based on distributed deep reinforcement learning for PEMFC air supply system," *IEEE Access*, vol. 9, pp. 7496–7507, 2021, doi: 10.1109/ACCESS.2021.3049162.

[4] Y. Li, Z. Zhou, X. Liu, and W.-T. Wu, "Modeling of PEM fuel cell with thin MEA under low humidity operating condition," *Appl. Energy*, vol. 242, pp. 1513–1527, May 2019, doi: 10.1016/j.apenergy.2019.03.189.

[5] W. R. W. Daud, R. E. Rosli, E. H. Majlan, S. A. A. Hamid, R. Mohamed, and T. Husaini, "PEM fuel cell system control: A review," *Renew. Energy*, vol. 113, pp. 620–638, Dec. 2017.
[6] A. S. Menesy, H. M. Sultan, A. Korashy, F. A. Banakhr, M. G. Ashmawy, and S. Kamel, "Effective parameter extraction of different polymer electrolyte membrane fuel cell stack models using a modified artificial ecosystem optimization algorithm," *IEEE Access*, vol. 8, pp. 31892–31909, 2020, doi: 10.1109/ACCESS.2020.2973351.
[7] D. Lu, F. Yi, D. Hu, J. Li, Q. Yang, and J. Wang, "Online optimization of energy management strategy for FCV control parameters considering dual power source lifespan decay synergy," *Appl. Energy*, vol. 348, Oct. 2023, Art. no. 121516.
[8] J. M. Cunningham, M. A. H. Man, and D. J. Friedman, "A comparison of high-pressure and low-pressure operation of PEM fuel cell systems," SAE Trans., America, Tech. Rep., 2001.
[9] Z. Deng, Q. Chen, L. Zhang, and Z. Fu, "Data driven NARMAX modeling for PEMFC air compressor," *Int. J. Hydrogen Energy*, vol. 45, no. 39, pp. 20321–20328, Aug. 2020, doi: 10.1016/j.ijhydene.2019.11.228.
[10] Z. Baroud, M. Benmiloud, A. Benalia, and C. Ocampo-Martinez, "Novel hybrid fuzzy-PID control scheme for air supply in PEM fuel-cell-based systems," *Int. J. Hydrogen Energy*, vol. 42, no. 15, pp. 10435–10447, Apr. 2017, doi: 10.1016/j.ijhydene.2017.01.014.
[11] C. Damour, M. Benne, C. Lebreton, J. Deseure, and B. Grondin-Perez, "Real-time implementation of a neural model-based self-tuning PID strategy for oxygen stoichiometry control in PEM fuel cell," *Int. J. Hydrogen Energy*, vol. 39, no. 24, pp. 12819–12825, Aug. 2014, doi: 10.1016/j.ijhydene.2014.06.039.
[12] A. Thomya and Y. Khunatorn, "Design of control system of hydrogen and oxygen flow rate for proton exchange membrane fuel cell using fuzzy logic controller," *Energy Proc.*, vol. 9, pp. 186–197, Jan. 2011, doi: 10.1016/j.egypro.2011.09.020.
[13] R. Yang, Z. Liu, and H. Su, "Control Lyapunov function based control strategy for air supply system of PEM fuel cells," in *Proc. 29th Chin. Control Decis. Conf. (CCDC)*, May 2017, pp. 1964–1969.
[14] M. A. Danzer, J. Wilhelm, H. Aschemann, and E. P. Hofer, "Model-based control of cathode pressure and oxygen excess ratio of a PEM fuel cell system," *J. Power Sources*, vol. 176, no. 2, pp. 515–522, Feb. 2008, doi: 10.1016/j.jpowsour.2007.08.049.
[15] Y. Li, P. Pei, Z. Ma, P. Ren, and H. Huang, "Analysis of air compression, progress of compressor and control for optimal energy efficiency in proton exchange membrane fuel cell," *Renew. Sustain. Energy Rev.*, vol. 133, Nov. 2020, Art. no. 110304.
[16] D. Stretch, B. Wright, M. Fortini, N. Fink, B. Ramadan, and W. Eybergen, "Roots air management system with integrated expander," USDOE Office Energy Efficiency Renew. Energy (EERE), America, Tech. Rep., 2016, doi: 10.2172/1325976.
[17] W. Yu, X. Sichuan, and H. Ni, "Air compressors for fuel cell vehicles: An systematic review," *SAE Int. J. Alternative Powertrains*, vol. 4, no. 1, pp. 115–122, Apr. 2015.
[18] Q. Li, P. Liu, X. Meng, G. Zhang, Y. Ai, and W. Chen, "Model prediction control-based energy management combining self-trending prediction and subset-searching algorithm for hydrogen electric multiple unit train," *IEEE Trans. Transport. Electrific.*, vol. 8, no. 2, pp. 2249–2260, Jun. 2022.
[19] Q. Li, L. Yin, H. Yang, T. Wang, Y. Qiu, and W. Chen, "Multiobjective optimization and data-driven constraint adaptive predictive control for efficient and stable operation of PEMFC system," *IEEE Trans. Ind. Electron.*, vol. 68, no. 12, pp. 12418–12429, Dec. 2021.
[20] I. Vaja and A. Gambarotta, "Internal combustion engine (ICE) bottoming with organic Rankine cycles (ORCs)," *Energy*, vol. 35, no. 2, pp. 1084–1093, Feb. 2010.
[21] D. M. Prater, "A dual cycle reciprocating engine," SAE, America, Tech. Paper, Aug. 2000, doi: 10.4271/2000-01-3070.
[22] F. Millo, F. Mallamo, E. Pautasso, and G. G. Mego, "The potential of electric exhaust gas turbocharging for HD diesel engines," SAE, America, Tech. Paper, 2006, doi: 10.4271/2006-01-0437.
[23] H. Lohse-Busch, K. Stutenberg, M. Duoba, X. Liu, A. Elgowainy, M. Wang, T. Wallner, B. Richard, and M. Christenson, "Automotive fuel cell stack and system efficiency and fuel consumption based on vehicle testing on a chassis dynamometer at minus 18 °C to positive 35 °C temperatures," *Int. J. Hydrogen Energy*, vol. 45, no. 1, pp. 861–872, Jan. 2020.
[24] M. A. Sheshpoli, S. S. M. Ajarostaghi, and M. A. Delavar, "Thermodynamic analysis of waste heat recovery from hybrid system of proton exchange membrane fuel cell and vapor compression refrigeration cycle by recuperative organic Rankine cycle," *J. Thermal Anal. Calorimetry*, vol. 135, no. 3, pp. 1699–1712, Feb. 2019.
[25] P. Pei, W. Yang, and P. Li, "Numerical prediction on an automotive fuel cell driving system," *Int. J. Hydrogen Energy*, vol. 31, no. 3, pp. 361–369, Mar. 2006.
[26] C. Wang, Z. Xing, S. Sun, W. Chen, and Z. He, "Experimental study on the performance of oil-free twin-screw expanders for recovering energy in fuel cell systems," *Appl. Thermal Eng.*, vol. 165, Jan. 2020, Art. no. 114613.
[27] W. Jiuxuan, Q. Mingxu, Z. Hong, and L. Xue, "Investigation on exhaust energy recovery system using radial turbine in high-power proton exchange membrane fuel cells," in *Proc. Turbo Expo, Powe Land, Sea, Air*, vol. 86052 2022, Art. no. V007T18A018.
[28] S. Martinez-Boggio, D. Di Blasio, T. Fletcher, R. Burke, A. García, and J. Monsalve-Serrano, "Optimization of the air loop system in a hydrogen fuel cell for vehicle application," *Energy Convers. Manag.*, vol. 283, May 2023, Art. no. 116911.
[29] L. Li, Q. Liang, J. Zhao, Y. Zhang, and Y. Liang, "Design and simulation of proton exchange membrane fuel cell exhaust gas recovery system," in *Proc. E3S Web Conf.*, vol. 186, 2020, p. 03007.
[30] Y. Shao, L. Xu, X. Zhao, J. Li, Z. Hu, C. Fang, J. Hu, D. Guo, and M. Ouyang, "Comparison of self-humidification effect on polymer electrolyte membrane fuel cell with anodic and cathodic exhaust gas recirculation," *Int. J. Hydrogen Energy*, vol. 45, no. 4, pp. 3108–3122, Jan. 2020.
[31] H. Chen, B. Liu, T. Zhang, and P. Pei, "Influencing sensitivities of critical operating parameters on PEMFC output performance and gas distribution quality under different electrical load conditions," *Appl. Energy*, vol. 255, Dec. 2019, Art. no. 113849.
[32] J. Jiao and F. Chen, "Humidity estimation of vehicle proton exchange membrane fuel cell under variable operating temperature based on adaptive sliding mode observation," *Appl. Energy*, vol. 313, May 2022, Art. no. 118779.
[33] T. Wittmann, S. Lück, C. Bode, and J. Friedrichs, "On the impact of condensation and liquid water on the radial turbine of a fuel cell turbocharger," *Machines*, vol. 10, no. 11, p. 1053, Nov. 2022.
[34] Q. Zhang, Z. Tong, S. Tong, and Z. Cheng, "Self-humidifying effect of air self-circulation system for proton exchange membrane fuel cell engines," *Renew. Energy*, vol. 164, pp. 1143–1155, Feb. 2021.
[35] X.-G. Yang, N. Burke, C.-Y. Wang, K. Tajiri, and K. Shinohara, "Simultaneous measurements of species and current distributions in a PEFC under low-humidity operation," *J. Electrochemical Soc.*, vol. 152, no. 4, p. 759, 2005.
[36] Z. P. Du, C. Steindl, S. Jakubek, and C. Hametner, "Concentration estimation for fuel cells: Design of experiments, nonlinear identification, and observer design with experimental validation," *IEEE Access*, vol. 11, pp. 10453–10470, 2023.
[37] H. Yuan, H. Dai, X. Wei, and P. Ming, "Model-based observers for internal states estimation and control of proton exchange membrane fuel cell system: A review," *J. Power Sources*, vol. 468, Aug. 2020, Art. no. 228376.
[38] J. T. Pukrushpan, A. G. Stefanopoulou, and H. Peng, *Control of Fuel Cell Power Systems: Principles, Modeling, Analysis and Feedback Design*. Berlin, Germany: Springer, 2004.
[39] J. T. Pukrushpan, A. G. Stefanopoulou, and H. Peng, "Control of fuel cell breathing," *IEEE Control Syst.*, vol. 24, no. 2, pp. 30–46, Apr. 2004.
[40] J. T. Pukrushpan, H. Peng, and A. G. Stefanopoulou, "Control-oriented modeling and analysis for automotive fuel cell systems," *J. Dyn. Syst., Meas., Control*, vol. 126, no. 1, pp. 14–25, Mar. 2004.
[41] J. Sun and I. V. Kolmanovsky, "Load governor for fuel cell oxygen starvation protection: A robust nonlinear reference governor approach," *IEEE Trans. Control Syst. Technol.*, vol. 13, no. 6, pp. 911–920, Nov. 2005.
[42] S. Gelfi, A. G. Stefanopoulou, J. T. Pukrushpan, and H. Peng, "Dynamics of low-pressure and high-pressure fuel cell air supply systems," in *Proc. Amer. Control Conf.*, 2003, pp. 2049–2054.
[43] R. Tirnovan and S. Giurgea, "Efficiency improvement of a PEMFC power source by optimization of the air management," *Int. J. Hydrogen Energy*, vol. 37, no. 9, pp. 7745–7756, May 2012.
[44] D. K. Kim, J. H. Seo, S. Kim, M. K. Lee, K. Y. Nam, H. H. Song, and M. S. Kim, "Efficiency improvement of a PEMFC system by applying a turbocharger," *Int. J. Hydrogen Energy*, vol. 39, no. 35, pp. 20139–20150, Dec. 2014.
[45] Z. Chen, H. Huang, T. Shi, X. Peng, and J. Feng, "Efficiency improvement and thermo-economic analysis of proton exchange membrane fuel cell system with energy recovery for both air and hydrogen," *Appl. Thermal Eng.*, vol. 233, Oct. 2023, Art. no. 121114.

[46] Z. Gong, B. Wang, Y. Xu, M. Ni, Q. Gao, Z. Hou, J. Cai, X. Gu, X. Yuan, and K. Jiao, "Adaptive optimization strategy of air supply for automotive polymer electrolyte membrane fuel cell in life cycle," *Appl. Energy*, vol. 325, Nov. 2022, Art. no. 119839.
[47] Q. Su, J. Zhou, F. Yi, D. Hu, D. Lu, G. Wu, C. Zhang, B. Deng, and D. Cao, "An intelligent control method for PEMFC air supply subsystem to optimize dynamic response performance," *Fuel*, vol. 361, Apr. 2024, Art. no. 130697.
[48] J. Tan, H. Hu, S. Liu, C. Chen, and D. Xuan, "Optimization of PEMFC system operating conditions based on neural network and PSO to achieve the best system performance," *Int. J. Hydrogen Energy*, vol. 47, no. 84, pp. 35790–35809, Oct. 2022.
[49] P. Wang, Y. Ma, J. Li, Y. Gao, Y. Zhang, and D. Ma, "A novel control algorithm of the air supply subsystem: Based on dynamic modeling of proton exchange membrane fuel cell," *Processes*, vol. 10, no. 8, p. 1499, Jul. 2022.

LIJIANG JIN received the bachelor's degree in electromechanical drainage and irrigation engineering from Yangzhou University, in June 1989, and the master's and Ph.D. degrees in management science and engineering from Jiangsu University, in 1999 and 2008, respectively.

He is currently with the School of Transportation, Zhenjiang College. His research interests include the optimization and control of ultra-high-speed air compressors for vehicle fuel cells and methods for improving the dynamic response performance of fuel cells.

JICHENG XU received the bachelor's degree in chemical education from Nanjing Normal University, in June 2002, and the Ph.D. degree in environmental engineering from Jiangsu University, in June 2016.

He is currently with Jiangsu Province Engineering Research Center of Surface Interface Functional Composites, Institute of Chemistry and Materials Science, Zhenjiang College. His research interest includes new hydrogen energy materials.

LINZHI WANG received the bachelor's degree in marketing from Jiangsu University, in June 2010, and the master's degree in management science and engineering from Jiangsu University, in June 2013.

She is currently with the School of Transportation, Zhenjiang College, engaged in cutting-edge technology research and marketing management of fuel cell vehicles.